

Solitary Wave Propagation in a Novel Granular Chain Setup

Bob Wei

February 11, 2017

Abstract

Mechanical energy transfer in granular materials has emerged as a topic of extensive study in recent years. Granular materials hold significance in various engineering applications such as energy localization and shock absorption. The work presented here focuses on the propagation of a bundle of non-dispersive energy, or a solitary wave (SW), in the granular chain, where the individual grains interact via the non-linear Hertz law. In this study, we capture the SW and measure its properties as it propagates through a novel experimental granular chain setup. This is facilitated by piezoelectric sensors and accelerometers embedded within the spherical grains. Our results indicate that the velocity of the solitary wave is dependent upon the material properties of the grains, which are characterized by the Young's modulus and Poisson's ratio. This provides experimental evidence that pulse propagation in granular media can be controlled by cleverly manipulating the material properties of the setup.

1 Introduction

The transfer of mechanical energy in systems comprised of macroscopic particles is a prominent area of theoretical and experimental study (refs) [1]. So-called granular materials are ubiquitous across many industries including mining and minerals processing, food production, construction, pharmaceuticals, and nanotechnology (refs). The research being conducted on granular systems, especially regarding the ability to control energy propagation within these systems, is important for a multitude of real-world applications.

This thesis focuses on the physics behind packed granular arrays or granular chains. The granular chain is a discrete, one-dimensional system of macroscopic particles usually composed of up to two different types of materials (refs); they are useful for many engineering applications related to shock absorption and energy localization. These systems are of particular interest due to the well established (refs) formation of a nondispersing bundle of energy, known as a solitary wave (SW), following an initial velocity perturbation to one end of an unloaded chain (no initial pre-compression). The SW propagates throughout the chain at a constant speed proportional to the amplitude of the wave (refs) or the bulk of the energy within the system. The SW also has a fixed width, that is characteristic of the grain shape, and is about five grain diameters in systems composed of spherical grains (refs).

$$\delta_{ij} = R_i + R_j - (x_j - x_i) \quad (1)$$

$$V_{ij} = a_{ij}\delta_{ij}^{5/2} \quad (2)$$

The formation of SW's is contingent on the highly nonlinear grain to grain interactions in the granular chain. This nonlinearity arises from the elliptical contact surfaces (refs) within an unloaded system of spherical grains. In particular, the contact potential be-

tween grains can be described by the nonlinear Hertz law, Eq. 2, where V_{ij} is the contact force between two grains (i and j), a_{ij} is the coefficient relating to grain material, δ_{ij} is the grain overlap calculated in Eq. 1, and $n = 5/2$ is the specific exponent for spherical grains.

Here we investigate the propagation and velocities with which these SW's travel throughout an unloaded granular chain. Our project goal has been to construct a novel, macroscopic model of the granular chain and the necessary apparatuses to be able to capture the solitary wave propagation. We are particularly interested in the effects of differing grain materials (varying hardness) on the velocity of the SW. Our data is also compared to that obtained from related simulations (refs) to further substantiate our results.

2 Experimental setup

In the experimental granular chain models, the grains used are standard at 12mm in diameter and are entirely composed of a single material: silicon nitride (mass = 2.090606g), borosilicate (mass = 2.02578g), stainless steel 420 (mass = 6.98721g), stainless steel 316 (mass = 7.19054g), or brass (mass = 7.50019g).

The main apparatus is designed as a hard-wall system (refs) that must be capable of holding each individual grain in a fixed position along the same central axis in order to maintain the unique contact potential responsible for SW propagation.

2.1 Initial apparatus

The initial experimental setup depicted in Figure 1 featured a trough-like design with two metallic plates attached diagonally to form a long V-shaped track. This design provides a means to support up to 25 spherical particles (12mm in diameter) in a 1D config-

uration, with each particle having two points of contact with the track system and capable of moving freely on the same horizontal axis. The inside of the metallic track is also covered in a layer of teflon (one strip on each of the two metal plates) in order to reduce the coefficient of friction in contact with the particles.

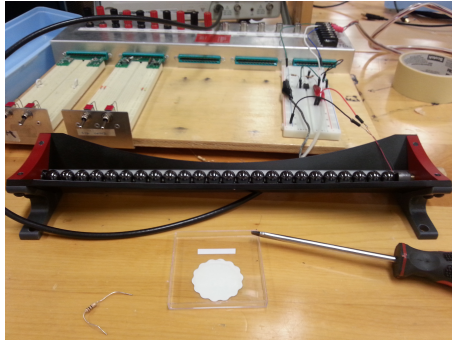


Figure 1: Side view of our initial experimental setup with 25 silicon nitride grains in place.

In the setup, the chain of particles is held between two hard metallic walls: with one end housing an adjustable screw that allows for the initial pre-compression in the system to be freely adjusted and the other end having a spherical cutout in the end wall that allows for an initial velocity perturbation to be applied to the system. The entire apparatus is bolted down to an optical table via four screws in order to minimize the effects of environmental vibrations.

This initial setup was plagued by frequent buckling throughout the chain, with particles often jumping out of alignment and compromising the 1D configuration. As noted by Boechler (refs), the point contact configuration of the granular chain is geometrically unstable, making the system prone to buckling when under higher loads. Thus, the experimental setup in Figure 1 was not used to collect data due to the frequent misalignment when a perturbation is applied to the chain.

2.2 Improved apparatus

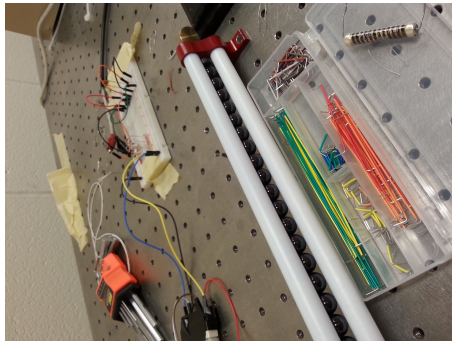


Figure 2: Our second experimental setup.

In order to prevent buckling, a second experimental setup, depicted in Figure 2, was designed and constructed. Like the previous setup, the entire apparatus is designed to be bolted down to an optical table and

implements a similar hard wall system, with an adjustable screw on one end and a spherical cutout on the other for providing an initial perturbation. However, the new track system responsible for fixing the grains in a 1D configuration is now composed of three teflon rods (teflon surface to reduce friction) aligned in an equilateral triangle configuration rather than the V-shaped trough design from the initial setup. With two horizontal rods for supporting the system of grains, a third rod can be implanted just above the grains so as to provide an upper barrier that prevents individual grains from buckling and becoming misaligned. With this new experimental setup, the grains are able to remain in an approximately 1D configuration even when a large static pre-compression or an initial perturbation.

This new setup is modeled after the experimental setup used by Boechler (refs) to test the vibrational response of statically compressed 1D granular crystals, which consists of four polycarbonate rods aligned in a square configuration. Likewise, Boechler implemented this configuration in order to keep the chain from buckling under high static loads.

2.3 Solenoid

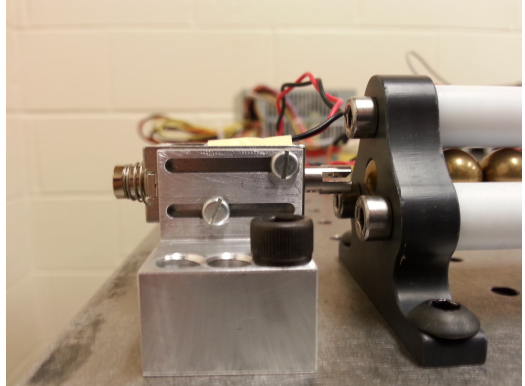


Figure 3: Side view of the solenoid setup with the contact arm retracted.

In order to provide the initial velocity perturbation needed to develop a SW, a solenoid, depicted in Figure 3 was used to consistently strike the left most grain in the granular chain. A solenoid was chosen over the piezoelectric actuators used in previous work (refs) as dynamic perturbations were unnecessary. The solenoid used is an open frame push type solenoid that functions with a pulse mechanism. The device is powered by 5VDC from a modified power supply unit and upon connecting the current, the arm of the solenoid extends outwards with a stroke length of 3.5mm.

As shown in Figure 3, the solenoid is attached to a mounting block that elevates the striking arm to the same height as the 1D granular chain. The spherical cutout in the left most wall of the experimental setup, mentioned in Section 2.2, allows for half of the end grain to protrude outwards, making a surface to which an initial perturbation can be applied. The mounting block also allows the solenoid to be adjusted horizon-

tally, providing a means to increase or decrease the amount of force with which the solenoid strikes the chain by changing the striking distance.

3 Methods

In order to capture and measure the SW in the experimental setup, sensors with high data capture rates needed to be placed inside of the chain. These specifications narrowed down the possible options to the piezoelectric sensor and the accelerometer due to their high sensitivities and small footprints. A laser Doppler vibrometer was also implemented successfully by Chong et al. (refs) to measure the dynamic responses of the chain to perturbations, though the necessary resources for such a setup were not available.

3.1 Piezoelectric sensor

Piezoelectric disks are capable of returning a voltage proportional to the force applied and this information can then be measured through an oscilloscope. The initial piezoelectric sensor used was the STEM-iNC SMD07T02R412WL model, which has a diameter of 7mm and a thickness of about 0.2mm (300 KHz resonant frequency, 3000 pF static capacitance). However, these sensors were very fragile and the ceramic disks cracked very easily due to their thickness and the nature of the grain-to-disk contact when inserted into the granular chain model (force is concentrated at a single point on the disk). In order to remedy this problem, the STEMiNC SMD10T2R111WL model was used, which is also ceramic but has a thickness of 2mm and a diameter of 10mm (1 MHz resonant frequency, 450 pF static capacitance).

3.1.1 Piezoelectric insert

An insertion mechanism for the piezoelectric sensor was proposed and designed in order to measure the force of the propagating SW at certain points in the granular chain. This design was partially inspired by the in-situ piezoelectric sensor used by Boehler (refs), in which the piezoelectric disk was epoxied between two halves of a particle in the granular chain. The design chosen, depicted in Figure 1, would ultimately consist of two semi-spheres machined from the same material as the corresponding grain (two models were constructed: brass and stainless steel 316). It was crucial that this machined model accurately mimicked the physical properties of an actual grain including the stiffness, mass, and dimensions in order to maintain the Hertz contact potential. Eventually, during experiments, the piezoelectric disk was sandwiched between the two semi-spheres by the compression force in the granular chain alone and not by epoxy. The mechanism is aligned in the granular chain in a way that preserves the spherical grain to grain contact.

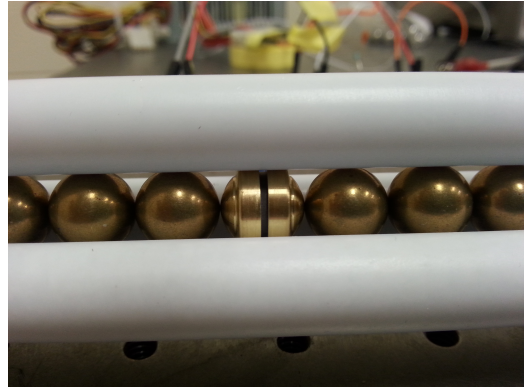


Figure 1: The piezoelectric insert mechanism for brass grains in the granular chain.

However, this mechanism was plagued by a few issues during data collection. When a light perturbation is applied throughout the granular chain, the piezoelectric insert was unable to detect any force upon contact and did not return a difference in voltage. It was determined that the machined mechanism damped the force acting on the sensor and that a very large initial impulse would be needed to initiate a response. Due to these problems, the piezoelectric insert was used sparingly in experiments, with some results being collected from a raw piezoelectric disk instead, which was inserted between two grains in the granular chain.

3.1.2 Data acquisition

Voltage signals from the piezoelectric sensor were measured by an oscilloscope (GW Instek GDS-1102A). The data is then transferred to a computer via a serial connection and is controlled by a Python interfacing script. However, the raw output from the piezoelectric sensor is highly unreliable due to the large amount of noise in the signal and must be passed through amplification and conditioning circuits.

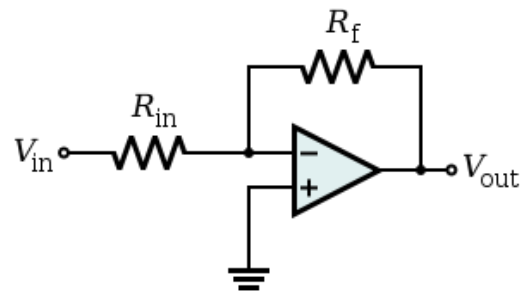


Figure 2: A basic schematic of the inverting amplification circuit used.

An inverting amplification circuit, similar to the one depicted in Figure 2, was tested and used to amplify the signal from the piezoelectric sensor. This circuit is mainly composed of an operational amplifier (TI-741) powered by + and - 12 V from a modified power supply and two different value resistors, R_f and R_{in} . The amplification provided by the operational amplifier is determined by the ratio of R_f/R_{in} . For

the piezoelectric signal, about a 10 times amplification was suitable and so resistance values of $R_f = 1 \text{ M}\Omega$ and $R_{in} = 100 \text{ K}\Omega$ were used. With this degree of amplification, the system signal-to-noise ratio was vastly improved. It must also be noted that the circuit causes the resulting voltage values from the piezoelectric sensor to be inverted.

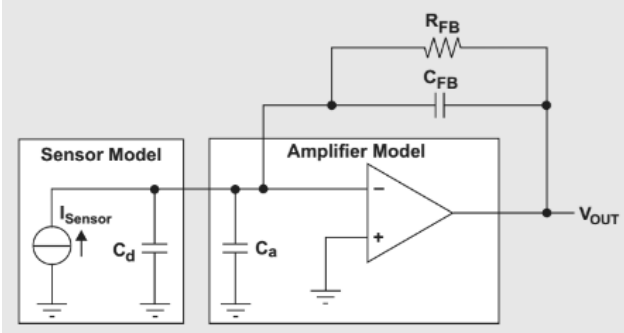


Figure 3: A basic schematic of the conditioning circuit used.

A conditioning circuit, similar to the one depicted in Figure 3, was also used to prepare the signal from the piezoelectric sensor for subsequent data analysis. This circuit provides control over the piezoelectric signal's lower cutoff frequency through the resistance value R_{FB} and the capacitance value C_{FB} .

$$F_L = \frac{1}{2\pi R_{FB} C_{FB}} \quad (1)$$

Following Eq. 1, the values for R_{FB} and C_{FB} can be adjusted to modify the lower cutoff frequency, F_L . Through trial and error, a resistance value of $100 \text{ M}\Omega$ for R_{FB} and a capacitance value of 1 nF for C_{FB} seemed to provide the highest signal-to-noise ratio, setting the lower cutoff frequency of the piezoelectric sensor to about 1.59 Hz . In addition to improving the signal, the conditioning circuit, particularly the arrangement of the operational amplifier, also inverted the voltage output. This build was used in many of the later experiments with the larger piezoelectric disk, replacing the previous amplification circuit.

3.1.3 Analysis of collected data

After obtaining the data from the oscilloscope via a PySerial connection, the digital data is saved as a file with two million voltage points as well as the corresponding two million data points. With this information, the piezoelectric signal can be processed and then analyzed. Initially, frequency analysis was conducted in Python using the Fast Fourier Transform (FFT) in order to further refine the piezoelectric sensor data. In this process, illustrated in Figure 4, an initial FFT was performed on the dataset, producing a frequency distribution from which the dominant frequencies can be manually removed (zeroed). After modification, an inverse FFT is performed on the dataset to produce a more refined reconstructed version of the initial data.

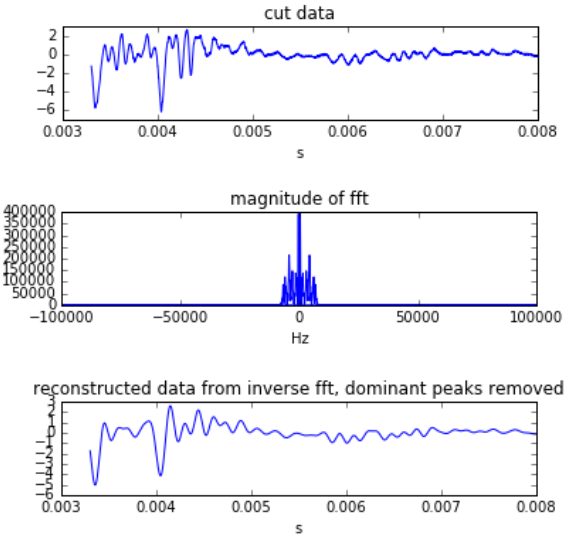


Figure 4: The frequency analysis process: (Top) the original distribution from the piezoelectric sensor, (Middle) the data after FFT and certain frequencies zeroed, (Bottom) the reconstructed distribution after inverse FFT.

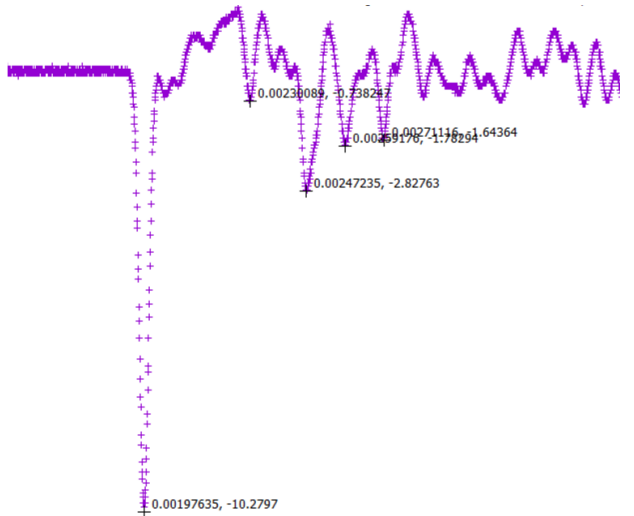


Figure 5: The data from the piezoelectric sensor plotted in GNUPlot. The time points at which the peaks occur are highlighted.

After processing the digital data, the new data file can be analyzed in order to provide information regarding the SW propagation in the granular chain. The datafile is plotted in GNUPlot software (as in figure 5), with the voltage points on the y-axis and the corresponding time points on the x-axis. With this graphical distribution, the peaks in the voltage signal (represents each time the SW reaches the piezoelectric sensor) can be identified and the time point at which they occur can also be determined accurately to ten nanoseconds. After ten trials under the same conditions, the time points for each peak (typically around three peaks can be identified) were then recorded in spreadsheet software and the average was taken in order to minimize the effects of random error.

$$if(P_n \text{ is odd}) : \quad t_{expected} = \frac{d(P_n - 1)}{v} \quad (2)$$

$$if(P_n \text{ is even}) : \quad t_{expected} = \frac{d(P_n - 2(x))}{v} \quad (3)$$

$$\text{Square difference} = (t_{observed} - t_{expected})^2 \quad (4)$$

Since the SW is known to propagate at a constant velocity v , a formula, illustrated in eqs. (2) and (3), can be developed to predict at what time, $t_{expected}$, the SW passes a certain point, x , in the granular chain, where $x = \frac{1}{4} \text{ chain}$ (between grains 6 and 7), $\frac{1}{2} \text{ chain}$ (between grains 12 and 13), $\frac{3}{4} \text{ chain}$ (between grains 18 and 19), or 1 full chain (between grain 24 and stiff end-wall). This formula provided a means to relate an actual experimental time point ($t_{observed}$) to a predicted time point ($t_{expected}$) and the disparity was quantified by the square difference calculated in equation 4. With the square difference for each position in the chain added together to form a total square difference and the horizontal distance spanned by the granular chain determined to be $d = 0.288\text{m}$ (24 grains \times 0.012m diameter for each grain), the spreadsheet solve tool was used to provide the value for the velocity that minimized the total square difference in the time points. This value of velocity in m/s was then compared to simulation data and ultimately used to form conclusions.

3.2 Accelerometer

Accelerometers are capable of measuring acceleration in the three dimensions and thus provide another method for capturing and measuring the solitary wave. In particular, the accelerometer model used is the ST Microelectronics LIS2HH12, which has a form factor of $2 \times 2 \times 1 \text{ mm}$ and is capable of measuring accelerations with output data rates of 10 Hz to 800 Hz.

3.2.1 Accelerometer insert

An insertion mechanism for the accelerometer, depicted in Figure 6, was proposed so that the small sensor could be implanted into the granular chain for measuring motion along the horizontal axis of the system. Since the accelerometer was initially attached to an adapter board (STEVAL-MKI164V1), the chip had to be removed and then reconnected to the capacitors on the board via very fine wires. The detached accelerometer was then inserted into the center of a drilled stainless steel 316 grain and was secured into place with epoxy. With this mechanism, the modified grain was then inserted into the granular chain and any SW perturbations within the chain could then be measured by the accelerometer.

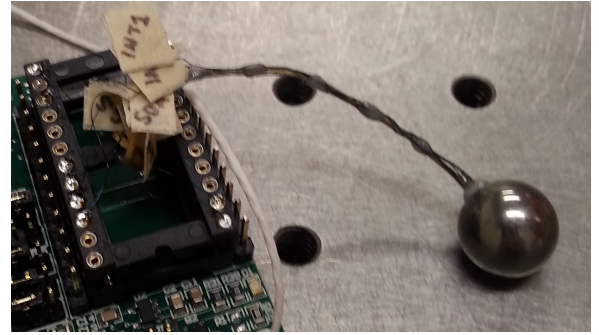


Figure 6: The accelerometer insertion mechanism with the adapter board and the accelerometer epoxied into the center of the stainless steel grain.

3.2.2 Accelerometer interfacing

As mentioned previously, the accelerometer is attached remotely to the STEVAL-MKI164V1 adapter board, which provides a channel for fast data evaluation. The adapter board itself is then directly connected to the DIL24 socket on the STEVAL-MKI109V2 motherboard (shown in Figure ref{fig:accelboard}), which provides USB 2.0 data transfer rates and allows for the accelerometer to be interfaced with a computer.

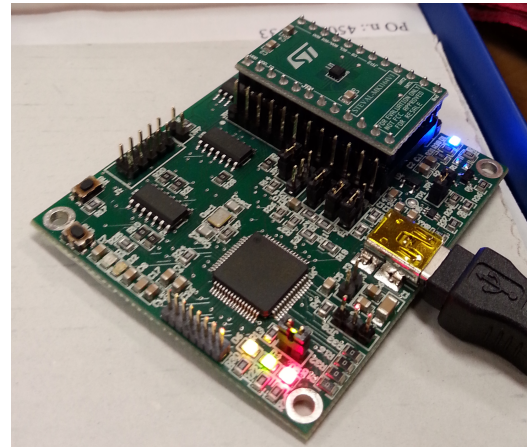


Figure 7: The adapter board (top right) attached to the STEVAL motherboard for data evaluation. The accelerometer is directly attached to the center of the adapter board in this image.

The software used to interface with the accelerometer was entirely developed in Python and utilized the PySerial package to establish a serial port connection. The three dimensional motion data obtained from the accelerometer was then parsed into three lists of data points (x, y, and z) and a separate list of corresponding time points.

3.2.3 Analysis of collected data

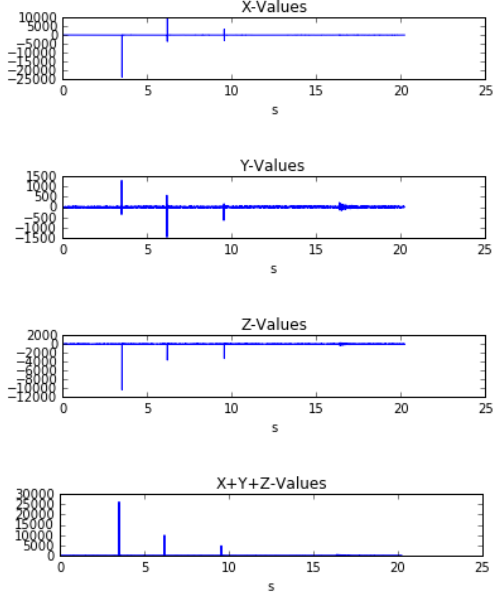


Figure 8: The three dimensional motion data from the accelerometer plotted in the IPython console using matplotlib. The peaks represent the SW propagation each time the system is perturbed (3 times).

After obtaining the data from the accelerometer, the three dimensional data points and the separate time points are plotted using Matplotlib in Python, as shown in Figure 8. In each of the four plots, the x-axis is marked by the time points in seconds while the y-axis is marked by the x, y, z, and x+y+z data points respectively. The x+y+z data is determined by adding each of the three components together via vector component addition.

However, as evident in Figure 8, the information provided in the plots were impossible to analyze due to the extremely poor resolution. The accelerometer was returning output data at a rate of 4000 data points in about 20 seconds which equates to about 200 Hz. Many adjustments were made to the interfacing Python script in order to speed up the data collection rate, however, the accelerometer never worked at above 200 Hz (despite the stated operating frequency of 10 to 800 Hz). This poor resolution rendered the data collected with the accelerometer to be useless in studying the SW propagation.

4 Numerical results

After initiating a velocity perturbation in the system from the leftmost grain at $t = 0$, the SW develops over several grains and proceeds to travel at a constant velocity through the granular chain. Due to the hardness of the end-walls, the SW reflects at each end of the chain with minimal time delay (refs) and continues to travel at the same velocity. Thus, as mentioned in Section 3.1.3: Analysis of collected data, the velocity of the SW can be determined from the piezoelectric

sensor data shown below based on the position of the sensor in the granular chain.

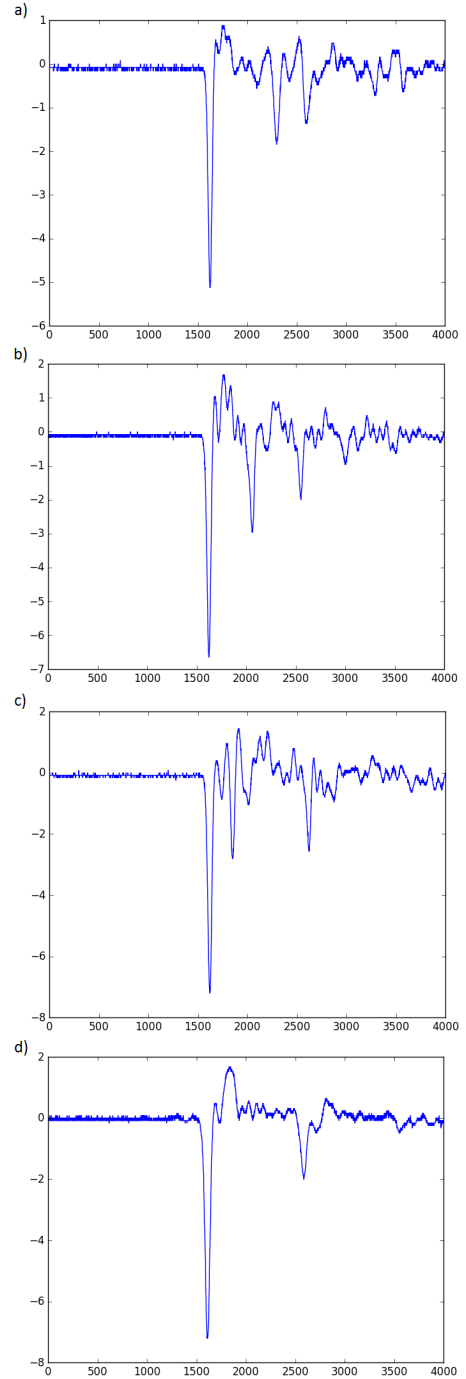


Figure 1: Piezoelectric sensor data plots with the peaks representing the SW propagation in a granular chain model composed of 24 borosilicate grains. The peaks clearly vary depending on the position of the piezoelectric sensor in the chain of 24 grains. Plot a): sensor between grains 6 and 7, Plot b) sensor between grains 12 and 13, Plot c) sensor between grains 18 and 19, Plot d) sensor between grain 24 and right end-wall.

The four plots in Figure 1 were recorded in a single experimental trial with borosilicate grains and subsequently, nine other identical trials were also recorded. The time points corresponding to each of the peaks in

the plots were then compiled in a spreadsheet and the average time points were calculated. These average time points were then used with the formulas mentioned in Section 3.1.3 to determine the velocity of the SW traveling through borosilicate grains, which was calculated to be 602.5844841 m/s.

This process was then repeated for the other four material types (stainless steel 420, stainless steel 316, brass, and silicon nitride) in order to determine the velocity of the SW when traveling in each of the different materials (listed below in Figure 2).

Actual Material	Velocity (m/s)
stainless steel 316	439.7371742
stainless steel 420	441.9787207
brass	351.7432348
borosilicate	602.5844841
silicon nitride	806.4340483

Figure 2: This table contains the calculated velocity of the solitary wave when traveling through grains composed of each of the five materials.

In order to better examine the relationship between SW velocity and material properties, the Young's modulus and Poisson's ratio were used to quantify the softness of each material. The softness of a material can be calculated through the following equations.

$$\text{softness} = \rho D \quad (1)$$

Where density ρ is calculated with the mass of a single grain in grams and radius ($r = 0.6$ cm) by

$$\rho = \frac{\text{mass of grain (g)}}{\frac{4}{3}\pi r^3} \quad (2)$$

And D is related to Young's modulus Y and Poisson's ratio σ of the consecutive grains i and j by

$$D_{ij} = \frac{3}{4} \left[\frac{1 - \sigma_i^2}{Y_i} - \frac{1 - \sigma_j^2}{Y_j} \right] \quad (3)$$

Since all of the grains in the chain were of the same material, i and j have identical properties and the equation 3 can be simplified to

$$D = \frac{3}{2} \left[\frac{1 - \sigma^2}{Y} \right] \quad (4)$$

With the equations above, the softness of each material was calculated using ρD , where a material becomes softer as ρD increases. The following figure illustrates the calculated ρD values for each of the five tested materials and it is clear that the materials, in order of increasing softness, are: silicon nitride, borosilicate, stainless steel 420, stainless steel 316, and brass.

Material	Density (g/cm ³)	Poisson ratio	Young Modulus (GPa)	Softness (ρD)
Stainless steel 420	7.723	0.28	200	0.053381376
Stainless steel 316	7.947	0.27	197.5	0.05595693949
Brass	8.29	0.31	113.5	0.09903080617
Borosilicate	2.239	0.2	64	0.0503775
Silicon nitride	3.211	0.27	310	0.01440444242

Figure 3: This table contains the calculated softness ρD of each of the five tested materials.

From figs. 2 and 3, one finds that the velocity of the SW v increases as the softness ρD decreases, meaning that the SW propagates faster through harder materials. Following this relationship, the SW travels fastest, at a velocity of 806.4340483 m/s, through silicon nitride grains and slowest, at a velocity of 351.7432348 m/s, through brass grains.

5 Comparison with simulations

The experimental data obtained was subsequently compared with that obtained from simulations (refs). In order to form a reasonable method for comparison, materials with similar softness values (ρD) to the five materials used in the experimental granular chain model were selected and used for comparing SW velocities. By comparing ρD values, the following materials shown in figure 1 were selected and paired together for comparison.

Simulation Material	Experimental Material
stainless steel	stainless steel 316
	stainless steel 420
red oak	brass
pyrex	borosilicate
boron carbide	silicon nitride

Figure 1: This table matches each experimental material with a comparable (in terms of ρD) material used in the simulations.

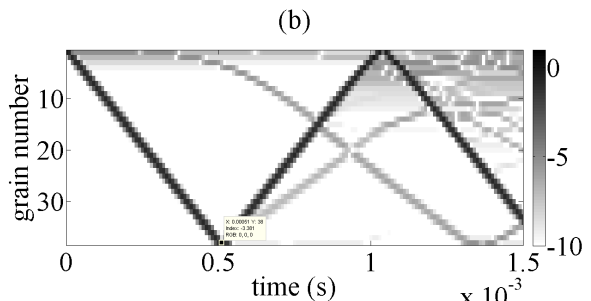


Figure 2: The kinetic energy density plot for boron carbide, depicting the presence of the system's kinetic energy stored in the SW.

The simulation data of the four materials above (stainless steel, red oak, pyrex, and boron carbide) were saved in their respective kinetic energy density plots, which depicted the location of the SW (a nondispersive bundle of kinetic energy) in the granular chain over time. It must be noted that the system in the simulations is composed of 38 grains rather than the 24 used in our experiments.

In Figure 2, the dark line represents the SW as it travels through the granular chain. As one can see, the time it takes for the SW to travel from grain 1 to grain 38 (for the line to go from top to bottom) is about 0.51 ms or about 0.00051 s. Each of the 38 grains in the simulation also has a diameter of 1.2 cm or 0.012 m. Therefore, with knowledge of both the distance traveled by the SW and the time taken to travel such a distance, one can calculate the velocity of the SW in the simulation as follows in Equation 1.

$$v = \frac{d(m)}{t(s)} \quad (1)$$

Where the distance traveled by the SW, d , can be determined by multiplying the number of grains in the chain by the diameter of each grain.

$$d = (38 \text{ spheres}) (0.012 \frac{m}{sphere}) = 0.456 \text{ m} \quad (2)$$

Using these calculations, the velocity of the SW as it travels in each simulation was determined and ultimately compared with the velocities of the SW in each corresponding experimental material.

Simulation Material	Velocity (m/s)	Experimental Material	Velocity (m/s)
stainless steel	414.5454545	stainless steel 316	439.7371742
		stainless steel 420	441.9787207
red oak	359.0551181	brass	351.7432348
pyrex	438.4615385	borosilicate	602.5844841
boron carbide	894.1176471	silicon nitride	806.4340483

Figure 3: This table compares the calculated velocities of the SW in the simulations to those calculated in the experimental trials.

From Figure 3, one finds that the measurements of the SW velocity in the experimental model generally agree with the corresponding measurements in the simulations. However, some discrepancies do exist between the experimental and simulation data, with the most notable one being the difference in SW velocity between brass (351.7432348 m/s) and red oak (359.0551181 m/s).

6 Conclusions

In this work, we have successfully constructed a novel experimental model of the granular chain capable of supporting up to 25 spherical grains within a hard-wall system. The setup was designed to preserve a 1D configuration as much as possible so that

the grains can interact consistently via the Hertz contact potential and thus allow for the formation of the SW following an initial perturbation. With the use of embedded piezoelectric sensors, we were then able to accurately capture and measure the SW as it propagated throughout the system and the velocities of the SW were obtained for grains of five different materials: stainless steel 316, stainless steel 420, borosilicate, brass, and silicon nitride.

A major finding from the results obtained in this study was the inverse relationship between SW velocity and the softness (ρD) of the grain material, where the velocity increased as the ρD value decreased. This relationship can be potentially exploited in a variety of engineering applications as a means to control the energy localization within granular media. In addition, our experimental results were further substantiated when compared to results from related simulations (refs).

However, there are still a number of unresolved problems within our experimental model and the fixing of such issues could be the basis for future work in granular media. The solenoid mechanism responsible for initially perturbing the system is controlled manually within the setup and necessary improvements could be made if connected to a micro-controller, providing a means to modify the way with which the solenoid strikes the chain. The in-situ piezoelectric insert could also be improved so as to improve its ability to measure the force. This could possibly be achieved by modifying the mechanism itself or by adjusting the piezoelectric conditioning circuit to better accommodate the output signal (i.e. different resistance and capacitance values). The accelerometer setup was also hampered by some problems as the output data was essentially unusable due to the low resolution and data collection rate. This problem could perhaps be remedied via the interfacing code, although an immediate solution would be to obtain an accelerometer model that supports much higher data capture frequencies.

References

- [1] V. F. Nesterenko. Nonlinear compression pulses in granular media. *J. Appl. Math. Tech. Phys.*, 1983.